

# The Origin of Fractal Distribution in Self-Gravitating Virialized System and Self-Organized Criticality

Yasuhide Sota<sup>1,3</sup> \*, Osamu Iguchi<sup>1</sup> \*\*, Masahiro Morikawa<sup>1</sup> †,  
 Takayuki Tatekawa<sup>2</sup> ‡‡ and Kei-ichi Maeda<sup>2,3,4</sup> ‡

<sup>1</sup> Department of Physics, Ochanomizu University, 2-1-1 Ohtuka, Bunkyo, Tokyo, 112-8610 Japan

<sup>2</sup> Department of Physics, Waseda University, Shinjuku, Tokyo 169-8555, Japan

<sup>3</sup> Advanced Research Institute for Science and Engineering, Waseda University,  
 Shinjuku, Tokyo 169-8555, Japan

<sup>4</sup> Advanced Institute for Complex Systems, Waseda University, Shinjuku, Tokyo 169-8555, Japan

## Abstract

Fractal structure and non-Gaussian velocity distribution are characteristic and universal properties in the self-gravitating virialized system such as galaxies or interstellar molecular clouds. Using one-dimensional ring model in which  $N$  particles constrained on a circular ring are interacting by three-dimensional (3-D) gravitating force, we examine the origin of these characteristic properties from the viewpoint of the gravitational phase transition. We find that a virialized state with negative specific heat appears at the intermediate energy scale, where a phase transition occurs and a cluster is formed. Classifying the particles in each state into three phases (core, halo and gas phases), we can characterize this virialized state by non-thermal property of the particles in *halo* phase. Although the relaxation time of the particles in the *core* phase is determined by the free-fall time, no typical time scale appears for the particles in the *halo* phase. As a result, the relaxation time of *halo* particles becomes very long comparing to that of *core* particles, then non-thermal properties are expected in a quasi-equilibrium state. In fact, non-Gaussian velocity distribution and fractal structure are found for *halo* particles. The fractal dimension is independent of the total energy. These results suggest that a scale free criticality in the gravitational interaction could be the main origin to cause the universal properties such as fractal structure and non-Gaussian velocity distribution in the 3-D self-gravitating system.

## I. INTRODUCTION

Astrophysical objects in our universe such as clusters of galaxies, galaxies, globular clusters and molecular clouds are composed of gravitationally interacting elements and are regarded as a self-gravitating system. Their statistical properties are characterized by the non-Gaussian velocity (or pair-wise velocity) distribution [1], the fractal structure in a configuration space [2], and the scaling relation between mass density and its size [3]. Since most of them are gravitationally virialized, gravity seems to play an important role in causing such statistical properties.

As for molecular clouds, the statistical properties such as Larson's scaling law [4], non-Gaussian velocity distribution and fractal structure in the iso-thermal contour [5] seem to be connected with the turbulence theory [6]. For example, Larson's law is likely to be explained by the Kolmogorov's theorem, since the

---

\*E-mail:sota@skyrose.phys.ocha.ac.jp

\*\*E-mail:osamu@phys.ocha.ac.jp

†E-mail:hiro@phys.ocha.ac.jp

‡‡E-mail:tatekawa@gravity.phys.waseda.ac.jp

‡E-mail:maeda@mse.waseda.ac.jp

exponent of the scaling law is almost the same as the value expected in the Kolmogorov theorem [7]. However, the turbulence theory itself is unsatisfactory, since there is no dynamical model leading to such a peculiar scaling law. In particular, when the component gas is strongly compressed and its self-gravity becomes important, we do not have any experimental data in contrast with the turbulence flow in the laboratory. Moreover, although the balance between energy injection and its dissipation plays an important role in such a universal law, it is not so clear if or not the observed molecular clouds or other astrophysical objects meet such a condition.

It may be important to invoke another possibility. There are so far several approaches to explain the fractal phenomena in self-gravitating system from the viewpoint of criticality and phase transition in gravito-thermo dynamics [8]. Strictly speaking, 3-D self-gravitational system cannot attain a stable equilibrium, because not only gravitational force is long range but also its potential diverges at origin. This causes the gravothermal catastrophe in the self-gravitating gas system enclosed by a solid adiabatic wall [9], [10], [11]. However, there may be a quasi-equilibrium state, which provide us a quasi-stable and important self-gravitating astrophysical object in the universe. In order to discuss such an equilibrium state, it is necessary to include a cutoff at small scale as well as at large scale. It is well known that 3-D gravitational system with the small scale cutoff has the state with a negative specific heat in the microcanonical state [12]. Although no gravothermal catastrophe occurs against the case without a cutoff, this system is highly unstable in the canonical state where the system is immersed in the heat bath. The system jumps from a gas state to a cluster state as the temperature goes down, which is just the first order phase transition.

So far several toy models have been proposed to study such statistical properties of 3-D gravitational system [13]. For example, the cell model and its extended version are among the simplest models to possess the property of phase transition, since the pair potential for the interaction takes the constant values both inside and outside the cells [14], [15]. At lower temperature, most particles are trapped in several clusters, while they escape and move freely at higher temperature in the model. However, it has the characteristic length scale of the cell size, against the scale-free 3-D gravitational system. On the other hand, 1-dim self-gravitating sheet model [16], [17], which has no characteristic length but no phase transition, is the antidote of this model. In these respects, these toy models are complementary, each other, but both of them are still missing to grasp the full nature of 3-D self-gravitating system. There are also several numerical analysis with the different type interactions including the effect corresponding to the lower and higher cutoffs [15], [18]. However, the value of the cutoff among these models seems too large to see the intrinsic properties of real 3-D gravitational model.

Here, we pay our attention to the dynamical aspects of the 3-D gravitational force on such a phase transition and examine the one-dimensional  $N$ -body ring model where particles constrained on a ring interact each other through 3-D gravitational force. We examine the case with the small cutoff and study the cutoff dependence on the statistical properties. We will show that the system approaches a quasi-equilibrium state independently of initial conditions and indicates the self-organized criticality (SOC) [19] known as the criticality which is free from the adjusting parameter in case with the small but finite value of cutoff parameter.

In section II, we will introduce our ring model, then classify the quasi-equilibrium states into three including the case with negative specific heat in section III. In sections IV, VI, and V, we analyze the particle motions from statistical point of view, and study the fractal structure of a formed cluster and see from our analysis how long it will take to relax the system. Finally, we will discuss our results in section VII.

## II. SELF-GRAVITATING RING MODEL

In this section, we introduce a self-gravitating ring (SGR) model, which is one-dimensional self-gravitating system and shows many interesting properties. As a one-dimensional self-gravitating system, so far, one-dimensional sheet model has mainly been analyzed in particular in the context of relaxation [17]. Although such a study has revealed many interesting properties of a self-gravitating system, some important features are still missing. Among them, phase transition, which appears in 3D self-gravitating system, is the most interesting issue to be addressed. Since the potential of the sheet model increases

linearly without an upper bound, there is no characteristic energy scale required for each particle to escape against gravitational binding energy, resulting that no phase transition will be expected.

Here we introduce another type of one-dimensional self-gravitating model which keeps some property of three-dimensional gravity and will show a phase transition. We consider one-dimensional self-gravitating  $N$  particles with mass  $m$ , whose motions are constrained on a circular ring with a fixed radius  $R$ . The force between each pair of particles is just the three dimensional gravitational interaction, whose distance is measured by a straight line in two dimensional Euclidean plane containing the ring.

We start with the physical Hamiltonian,

$$H_{\text{phys}} = \frac{1}{2mR^2} \sum_{i=1}^N P_i^2 - \sum_{i < j}^N \frac{Gm^2}{\sqrt{2}R\sqrt{1 - \cos(\theta_i - \theta_j) + \epsilon}}. \quad (2.1)$$

where the position of  $i$ -th particle constrained on the ring is described only by an angular variable  $\theta_i$  as  $\mathbf{r}_i = (R \sin \theta_i, R \cos \theta_i)$ , and  $\epsilon$  is a cutoff parameter and the momentum  $P_i$  conjugate to  $\theta_i$  is given by  $P_i = mR^2 d\theta_i/dt$ . The gravitational interaction vanishes because of this cutoff, if the distance of two particles is smaller than the scale length  $\xi \equiv \sqrt{2\epsilon}R$ .

For our numerical simulation, we shall introduce dimensionless variables as follows: The physical Hamiltonian (2.1) can be rescaled as

$$H_{\text{phys}} = Gm^2 \frac{N}{R} H, \quad (2.2)$$

where

$$H = \frac{1}{2} \sum_{i=1}^N p_i^2 - \sum_{i < j}^N \frac{1}{\sqrt{2N}\sqrt{1 - \cos \theta_{ij} + \epsilon}}. \quad (2.3)$$

Here a dimensionless momentum  $p_i$  is defined by  $p_i = d\theta/d\tau$  and a new time coordinate  $\tau$  is introduced as  $\tau \equiv t/t_{\text{dyn}}$ .  $t_{\text{dyn}}$  is a characteristic dynamical time of the present system defined by

$$t_{\text{dyn}} \equiv \sqrt{\frac{R^3}{GNm}} \sim \frac{1}{\sqrt{G\bar{\rho}}}, \quad (2.4)$$

where  $\bar{\rho}$  is a mean density of our system.  $t_{\text{dyn}}$  denotes a time scale of a particle going around the ring. Therefore, in order to study thermodynamical properties of a quasi-equilibrium state, if it exists, it is necessary to simulate the system for much longer time duration as  $t > t_{\text{dyn}}$ . Here we have numerically solved the present model with a symplectic integrator [22], by which the total Hamiltonian is conserved with a quite high accuracy, even after a long time-interval of numerical simulation.

When a cluster is formed, we find another typical time scale  $t_{\text{cl-dyn}}$ , which is a dynamical time scale of the formed cluster and is different from  $t_{\text{dyn}}$ . This is just because the mass density in the cluster is much larger than that of a gaseous phase, i.e.  $t_{\text{cl-dyn}}$  is estimated by

$$t_{\text{cl-dyn}} = \sqrt{\frac{1}{G\rho_{\text{cl}}}} \sim \sqrt{\frac{d_{\text{cl}}^3}{GNm}}, \quad (2.5)$$

where  $\rho_{\text{cl}}$  and  $d_{\text{cl}}$  are a mass density of a cluster and a cluster size, respectively. Although  $t_{\text{dyn}}$  is independent of a cutoff parameter  $\xi$ , the dynamical time  $t_{\text{cl-dyn}}$  may depend implicitly on  $\xi$  because  $d_{\text{cl}}$  is related to  $\xi$  (see §. III, and §. IV). Note that we will classify the particles with three phases, *core* phase, *halo* and *gas* phases in the next section and show that the above sort of typical time scale is applicable only for the particles in the *core* phase, but not for the *halo* phase.

As we see from (2.2), if we do not change the number density in the ring, i.e. if  $N/R$  is fixed, the present model is equivalent to the model defined by the Hamiltonian (2.3), then the properties are essentially determined by a particle number  $N$  and a cutoff parameter  $\epsilon$ . It should also be stressed that the present model (2.3) keeps extensiveness of the system.

Taking the lowest Fourier mode from the Fourier expansion of the potential of this model, we find a well-known one-dimensional ring model, called the Hamilton mean field (HMF) model [21]. Then the SGR model is the similar to the HMF model in the limit of  $\epsilon \rightarrow 1$  because the curvature of the potential at  $\theta = 0$  is almost the same as that at  $\theta = \pi$ , while it recovers the exact 3-D gravity in the limit of  $\epsilon \rightarrow 0$ .

In this paper, we fix the total number of particles to  $N = 100$ . Then, only the cutoff parameter  $\epsilon$  is a parameter which determines all properties. In the next section, we numerically examine the statistical aspects of the SGR model and compare them with the results of the HMF model.

### III. CLASSIFICATION OF PARTICLES

Here, we study the properties of "equilibrium" state in SGR model. Since the present system includes a state with a negative specific heat as is shown below, there is no thermal equilibrium state in a usual sense. Hence we use "equilibrium" for a stationary or quasi-equilibrium state, which is sometimes found as a kind of transient attractor for a certain time period.

#### A. Negative specific heat

First we present a relation between the temperature and the internal energy, i.e. the  $T$ - $U$  relation in Fig.1. The temperature  $T$  and the internal energy per one particle  $U$  of the present system are defined by

$$T = \frac{2 \langle K(t) \rangle}{N} , \quad (3.1)$$

$$U = \frac{H}{N} , \quad (3.2)$$

where  $K(t)$  is the kinetic energy of the system at time  $t$  and  $\langle K(t) \rangle$  denotes its time averaging from initial time to  $t$ . The internal energy  $U$  is conserved in the present microcanonical system.

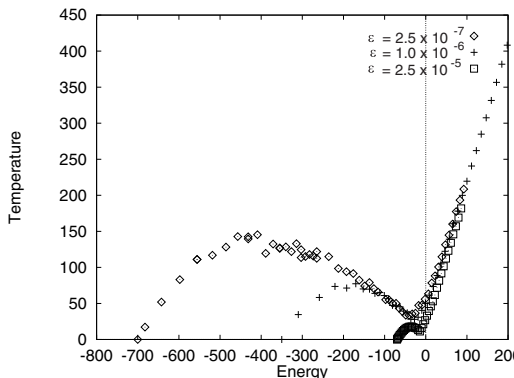


FIG. 1. Temperature  $T$  vs energy per one particle  $U$  in the case of  $\epsilon = 2.5 \times 10^{-5}$ ,  $1.0 \times 10^{-6}$ , and  $2.5 \times 10^{-7}$ . In each  $T$ - $U$  curve, there are two critical energy scales;  $U_{\text{c-low}}(\epsilon)$  and  $U_{\text{c-high}}(\epsilon)$ , between which a negative specific heat appears. In this range, there seems to exist an asymptotic line of  $T = -0.38U$  in the limit of  $\epsilon \rightarrow 0$ .

From Fig.1, we find two critical energy scales;  $U_{\text{c-low}}(\epsilon)$  and  $U_{\text{c-high}}(\epsilon)$  in this  $T$ - $U$  curve. The energy scale  $U_{\text{c-high}}(\epsilon)$  corresponds to a mean gravitational binding energy per one particle, which is estimated as  $\langle -1/(\sqrt{2}N\sqrt{1 - \cos\theta} + \epsilon) \rangle \times (N(N-1)/2)/N \sim -0.5$ , while,  $U_{\text{c-low}}(\epsilon)$  strongly depends on a cutoff  $\epsilon$ , e.g.  $U_{\text{c-low}}(\epsilon) \sim -400.0$  and  $-40$  for  $\epsilon = 2.5 \times 10^{-7}$  and  $\epsilon = 2.5 \times 10^{-5}$ , respectively.

In the energy range between these two energy scale, i.e.  $U_{\text{c-low}}(\epsilon) < U < U_{\text{c-high}}(\epsilon)$ , the system has a negative specific heat. This existence of a negative specific heat may correspond to an appearance of a kind of phase transition [12], [14], [15], [18]. Once energy is injected into a part of the system from

the outer region, then its temperature decreases because of a negative specific heat. Then we expect a cluster formation through this catastrophic instability. Such a phase transition from a gaseous state to a cluster state in fact appears and a variety structure will be realized in the intermediate energy range with a negative specific heat (see below).

### B. Three states: gaseous ( $\mathcal{G}$ -), virialized ( $\mathcal{V}$ -), and condensed ( $\mathcal{C}$ -) states

Using the above two critical energy scales,  $U_{\text{c-low}}(\epsilon)$  and  $U_{\text{c-high}}(\epsilon)$ , we shall classify the present equilibrium state into three as follows:

First, we call a region with an energy higher than  $U_{\text{c-high}}(\epsilon)$ , i.e. a high energy region with a positive specific heat, a gaseous state ( $\mathcal{G}$  -state). This is because almost all particles in this state have much higher energy than the gravitational binding energy and are moving freely. This  $\mathcal{G}$  -state is stable because of the existence of the infrared cutoff ( $\theta \leq 2\pi$ , or a largest physical scale  $\sim R$ ).

Secondly, for the energy lower than  $U_{\text{c-low}}(\epsilon)$ , there is also a region with a positive specific heat, which we shall call a condensed state ( $\mathcal{C}$  -state). In this state, most particles are gathering in one cluster. This  $\mathcal{C}$  -state is also stable because of the existence of the ultraviolet cutoff  $\epsilon$ .

The last but not the least, there exists an intermediate state with a negative specific heat between  $U_{\text{c-low}}(\epsilon)$  and  $U_{\text{c-high}}(\epsilon)$ , which we call a virialized state ( $\mathcal{V}$  -state).

This is because most particles are gravitationally bounded and if the system is virialized (we expect so), its specific heat will become negative from the gravitationally virialized condition. This  $\mathcal{V}$  -state seems to satisfy a virial condition, i.e.  $\langle K \rangle = -c_{\text{virial}} \langle V \rangle$  with  $c_{\text{virial}} = 0.16$  from the slope of  $\mathcal{V}$  state in Fig.1. Note that  $c_{\text{virial}} = 1/2$  for the virial state in 3D gravity. Since this slope is almost independent of the cutoff parameter, we believe that this  $\mathcal{V}$  -state has the same intrinsic properties as those in real 3D gravity.

This is in contrast with the HMF model, in which only  $\mathcal{G}$  - and  $\mathcal{C}$  -states appear, and then a second order phase transition occurs. On the other hand, the present  $\mathcal{V}$  -state appearing in the SGR model becomes strongly unstable, if the system is immersed in a heat bath. Then a first order phase transition will occur in the SGR model for a canonical ensemble. In the limit of  $\epsilon \rightarrow 0$ , that is for a realistic gravity, the range of the  $\mathcal{V}$  -state gets sensitively wider and eventually diverges. Therefore, such a phase transition turns out to be scale-independent. As for the sheet model, only  $\mathcal{C}$  -state exists because the system has no characteristic energy scale, and then there is no phase transition.

### C. Three phases: *gas* , *halo* , and *core* phases

To get more information, in particular about a phase space structure, we shall define three phases in each “equilibrium” state. That is, we divide all particles into the *core* phase, *halo* phase, and *gas* phase by the above two critical energy scales,  $U_{\text{c-low}}(\epsilon)$  and  $U_{\text{c-high}}(\epsilon)$ . The total energy of  $i$ ’th particle is defined as

$$E_i \equiv \frac{1}{2}p_i^2 - \sum_{j \neq i}^N \frac{1}{\sqrt{2}N\sqrt{1 - \cos\theta_{ij} + \epsilon}}. \quad (3.3)$$

The *core* , *halo* , and *gas* phases are defined by the particles with the energy of  $E_i < U_{\text{c-low}}(\epsilon)$ , those with the energy of  $U_{\text{c-low}}(\epsilon) < E_i < U_{\text{c-high}}(\epsilon)$ , and those with the energy of  $E_i > U_{\text{c-high}}(\epsilon)$ , respectively. Note that even for the  $\mathcal{C}$  -state, there exist a few particles in the *gas* phase. A group of particles either in *core* phase or in *halo* phase is called a cluster in this paper because those make one bound state.

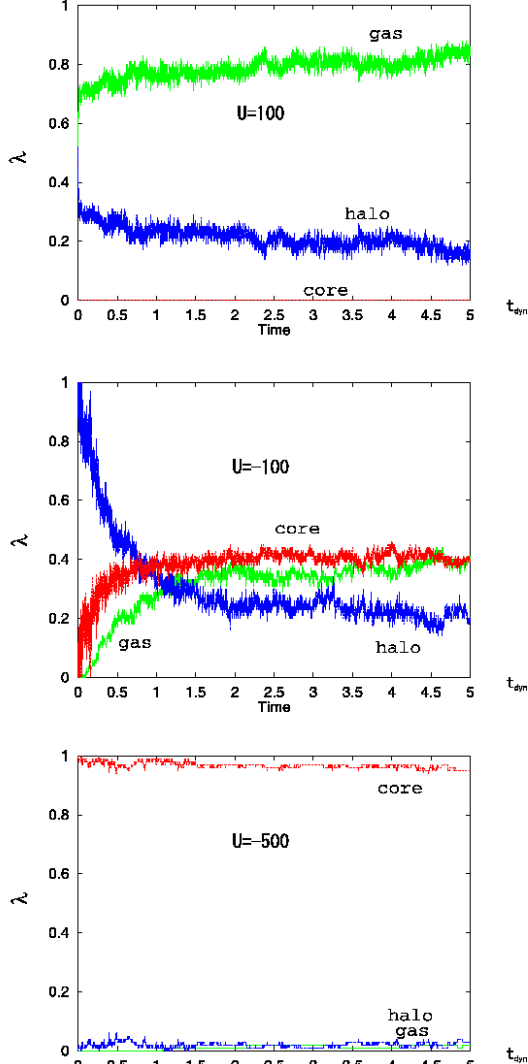


FIG. 2. The time evolution of the ratio of each phase;  $\lambda_{\text{core}}$ ,  $\lambda_{\text{halo}}$ , and  $\lambda_{\text{gas}}$  in  $\mathcal{G}$ -state (top), in  $\mathcal{V}$ -state (middle), and in  $\mathcal{C}$ -state (bottom) for  $\epsilon = 2.5 \times 10^{-7}$ . In  $\mathcal{G}$ -state, gas particles dominate, although there is still small part of *halo* particles. While, in  $\mathcal{C}$ -state, most particles are in *core* phase. In the  $\mathcal{V}$ -state, however, many particles experience at least two phases. Some particles wander from one phase to another in three phases.

In SGR model, the ‘‘equilibrium’’ state at very low temperature is inhomogeneous and one cluster exists. Most particles are condensed in *core* phase, resulting that its total potential becomes deep. A few particles in *halo* phase are going around this *core* particles, that is, a few particles are going around many particles in the cluster. As the temperature gets higher, the ratio of *halo* particles to *core* particles increases. Increasing the temperature further, there also appears a *gas* phase where some particles evaporate from the cluster and are going around the ring. At very high temperature, all particles will move freely.

We describe the relative ratios of particle number in each phase by  $\lambda_{\text{core}}$ ,  $\lambda_{\text{halo}}$ , and  $\lambda_{\text{gas}}$ , which satisfies the particle number conservation condition,

$$\lambda_{\text{core}} + \lambda_{\text{halo}} + \lambda_{\text{gas}} = 1. \quad (3.4)$$

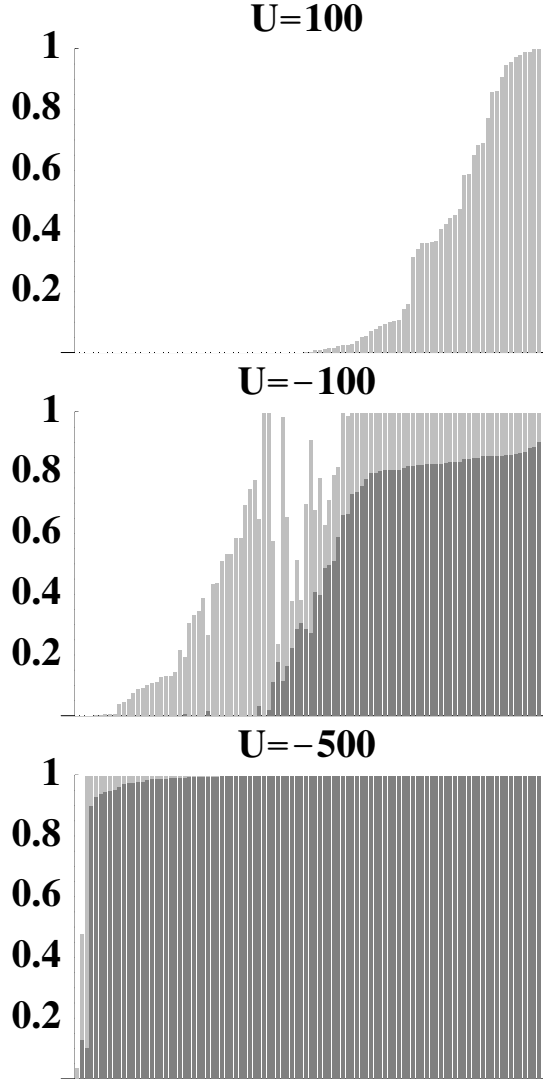


FIG. 3. The relative ratio of time intervals of three phases in which each particle stays until  $t = 5t_{\text{dyn}}$ . The each point in the horizontal axis corresponds to each particle, and each ratio of *gas* , *halo* , and *core* phase is represented by white, gray, and black region, respectively.

We show the time evolution of  $\lambda_{\text{core}}$ ,  $\lambda_{\text{halo}}$ , and  $\lambda_{\text{gas}}$  in Fig.2 for the case of  $\epsilon = 2.5 \times 10^{-7}$ . From these figures, these ratios approach the asymptotic value beyond  $t \sim t_{\text{dyn}}$ , in fact,  $\lambda_{\text{core}} \sim 0$ ,  $\lambda_{\text{halo}} \sim 0.2$ , and  $\lambda_{\text{gas}} \sim 0.8$  for  $U = 100$  ( $\mathcal{G}$  -state),  $\lambda_{\text{core}} \sim 0.41$ ,  $\lambda_{\text{halo}} \sim 0.23$ , and  $\lambda_{\text{gas}} \sim 0.36$  for  $U = -100$  ( $\mathcal{V}$  -state),  $\lambda_{\text{core}} \sim 0.96$ ,  $\lambda_{\text{halo}} \sim 0.02$ , and  $\lambda_{\text{gas}} \sim 0.02$  for  $U = -500$  ( $\mathcal{C}$  -state). We could naively claim that three phases coexist only in the  $\mathcal{V}$  -state.

In Fig.3, the relative ratio of time intervals of three phases in which each particle stays until  $t = 5t_{\text{dyn}}$  is shown. As we expect, in both  $\mathcal{G}$  - and  $\mathcal{C}$  -states, most particles stay just in one phase for a quite long time. For the  $\mathcal{V}$  -state, however, many particles experience at least two phases. Some particles wander from one phase to another in three phases.

## IV. PARTICLE MOTIONS

Here we shall examine particle motions in each state. As we discussed in §. II, there are two dynamical time scales;  $t_{\text{dyn}}$  and  $t_{\text{cl-dyn}}$ . The dynamical time scale  $t_{\text{cl-dyn}}$  is estimated by the averaged time of one oscillation of particles. This time is consistent with the formula (2.5) if  $d_{\text{cl}} \sim (30-70) \times \epsilon$ , which has been confirmed by a particle distribution. Then,  $t_{\text{cl-dyn}}$  strongly depends on a cutoff, i.e.  $t_{\text{cl-dyn}} \sim 0.004t_{\text{dyn}}$  for  $\epsilon = 2.5 \times 10^{-7}$ , and  $t_{\text{cl-dyn}} \sim 10t_{\text{dyn}}$  for  $\epsilon = 2.5 \times 10^{-3}$ .

### A. Velocity distribution

In Fig.4, we show the distribution of the particle velocities observed every unit time ( $t_{\text{dyn}}$ ) from  $t = 1t_{\text{dyn}}$  to  $t = 5t_{\text{dyn}}$ . We have simulated ten models with different initial data for a given energy. Then the size of data for one velocity distribution is 5000 for each model.

First we depict the velocity distributions for the clusters both in the  $\mathcal{C}$ -state and  $\mathcal{V}$ -state. The distribution is almost Gaussian for the  $\mathcal{C}$ -state, but that for  $\mathcal{V}$ -state is not exactly Gaussian but has an apparent tail. In order to clarify the origin of this tail, we show the distributions of the *halo* and *core* particles separately in Fig.4. We find that the distribution of the *core* particles is always Gaussian, i.e.

$$P(v) = \frac{1}{\sqrt{2\pi}\sigma} e^{-\frac{v^2}{2\sigma^2}}, \quad (4.1)$$

with the dispersion  $\langle v_{\text{core}}^2 \rangle^{1/2} \equiv \sigma = 7.29$  and  $10.9$  in  $\mathcal{V}$ - and in  $\mathcal{C}$ -states, respectively, while the distribution of the *halo* particles is non-Gaussian in Fig. 4.

As for the distribution of *halo* particles, we may be able to explain it as follows: For a stable or quasi-stable state in a self-gravitating system, we may well expect that a virial equilibrium is established, i.e.

$$\langle K_{\text{phys}} \rangle = -c_{\text{virial}} \langle V_{\text{phys}} \rangle, \quad (4.2)$$

where  $\langle K_{\text{phys}} \rangle$  and  $\langle V_{\text{phys}} \rangle$  are an averaged kinetic energy and a potential energy in the physical system, respectively.  $C_{\text{virial}}$  is a constant and is equal to  $1/2$  for real 3D self-gravitating system. For  $N$ -particle system of two-body interacting particles,  $\langle V_{\text{phys}} \rangle \propto N^2$ . From the virial theorem, we find that the averaged velocity dispersion is given as

$$\langle v_{\text{phys}}^2 \rangle_{N-\text{particle}} \propto \langle K_{\text{phys}} \rangle / N \propto N, \quad (4.3)$$

which means that the kinetic energy is not extensive, and then the conventional Boltzmann statistics is no longer valid.

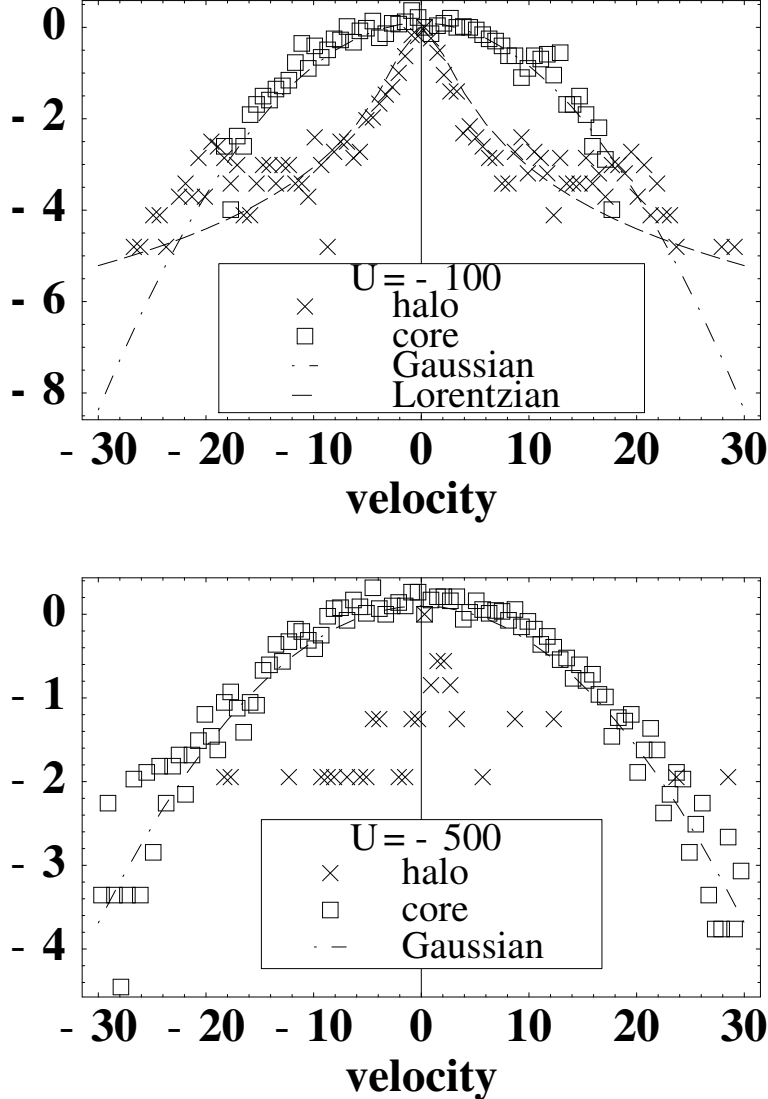


FIG. 4. The linear-log plot of velocity distribution of particles in each phase by use of data taken every unit time ( $t_{\text{dyn}}$ ) from  $1t_{\text{dyn}}$  to  $5t_{\text{dyn}}$  and superposed. For the *core* particles in  $\mathcal{V}$ -state and  $\mathcal{C}$ -state, the Gaussian distribution with  $\sigma = 7.29$  and  $10.9$  fit well, respectively. On the other hand, for the *halo* particles in  $\mathcal{V}$ -state, we find the Lorentzian distribution ( $\alpha = 1$ ) with  $s = 2.2$  is consistent with our numerical result.

It is well known that the asymptotic distribution as a consequence of the central-limit theorem is not restricted to be the Gaussian, provided we do not require the finiteness of the dispersion. This asymptotic distribution is defined to be

$$\sum_{i=1}^N x_i \stackrel{d}{=} N^{1/\alpha} x, \quad (4.4)$$

where  $\stackrel{d}{=}$  means that both sides are equal as distributions. Here,  $x_i$  and  $x$  are the same probabilistic variables for  $N$ -particle system and for one-particle system, respectively. If we apply this to the velocity distribution, this distribution shows a non-extensive property,

$$\langle v^2 \rangle_{N-\text{particle}} = N^{2/\alpha-1} \langle v^2 \rangle_{\text{one-particle}} \quad (4.5)$$

in general. A generalized central-limit theorem guarantees that the stable configuration exists for  $0 < \alpha \leq 2$  and the distribution is explicitly given by [20]

$$P(v) = \frac{1}{2\pi} \int_{-\infty}^{\infty} dy \exp[-ivy - s|y|^{\alpha}]. \quad (4.6)$$

From (4.3), we find that  $\alpha = 1$  and the distribution reduces to

$$P(v) = \frac{1}{\pi} \frac{s}{v^2 + s^2}. \quad (4.7)$$

Note that if the kinetic energy is extensive, we find that  $\alpha = 2$ , resulting in the Gaussian distribution (4.1) with  $\sigma = \sqrt{2s}$ .

Now we assume the  $\mathcal{V}$ -state in our model is also in a virial equilibrium, i.e.  $\langle K_{\text{phys}} \rangle = -c_{\text{virial}} \langle V_{\text{phys}} \rangle$  in the physical system. Since  $\langle V_{\text{phys}} \rangle \sim N^2$ ,  $\langle K_{\text{phys}} \rangle \sim N^2$ . Although we have simulated a dimensionless model (2.3) with a normalized time  $\tau$ , we find a relation

$$\langle K \rangle \sim \frac{t_{\text{dyn}}^2}{R^2} \langle K_{\text{phys}} \rangle \sim \frac{R}{N} \times N^2 \sim N^2 \quad (4.8)$$

because the equivalence between two systems is guaranteed if the number density  $N/R$  is fixed. Then we find the same index of  $\alpha = 1$  for our present numerical model as well. We show the distribution (4.7) with  $s = 2.2$  in Fig. 4(b), which is consistent with our numerical result. The parameter  $s$  is thought to be a generalized temperature. Since this non-Gaussian distribution is closely related to the existence of the virial equilibrium, it may be that the distribution (4.7) is a characteristic and universal one in a self-gravitating system.

Since the SGR model is a Hamiltonian system, the entropy is conserved for all time. Even if it takes a long time to evolve, the system never reaches a maximal entropy state. Of course, taking a long time average, any ordinary system, whose phase space is compact, will relax and the velocity distribution becomes Gaussian. In fact, as for the sheet model and the HMF model, the velocity distribution becomes Gaussian at least at  $t \sim \mathcal{O}(10^4)t_{\text{micro}}$  for the sheet model, where  $t_{\text{micro}} \equiv \sqrt{L^3/GNm}$  with  $L$  being a scale of the system, and at  $t \sim \mathcal{O}(10^3)t_{\text{dyn}}$  for the HMF model. However, the above results about velocity distribution seem to imply that the existence of *halo* particles keeps the system from attaining the thermal-equilibrium state as a whole in  $\mathcal{V}$  state. We will discuss this more in §.VI. Here, we study the motion of *halo* particles in detail because those are not described by a Gaussian distribution.

## B. Recurrent motion of halo particles

The peculiar motion of the particles is observed in the HMF model [23]. At the state near the critical energy, Lévy-type flight and anomalous diffusion appear. Those behaviors are caused by particle transition between *core* phase and *gas* phase. Such peculiar behaviors, however, may come not from a long range force itself but rather from a periodicity of the configuration space. In fact, for all Lévy-type flight numerically shown in the HMF model, any flight distance is longer than  $2\pi$ . Since our SGR system is also a closed ring, we may have a similar flight motion. However, here we will pay our attention to the recurrent motion of the particles, especially of the *halo* particles and will reveal a universal property in the motion of *halo* particles in  $\mathcal{V}$ -state (or even in  $\mathcal{C}$ -state). Note that the energy range we will discuss is much wider than that for the above Lévy-type flight motion in the HMF model, because our result can be applied to all  $\mathcal{V}$ -state, while the latter case is found only near the critical energy. When  $\epsilon \rightarrow 0$ , the range becomes much wider, and then we believe that our result is valid also for real 3D gravity as well.

First, we show that the particles in the *core* phase move regularly around the center of the cluster, whose period of the oscillation is approximated by the free-fall time determined by the density of the cluster,  $t_{\text{cl-dyn}}$ . On the other hand, the *halo* particles seem to move around the cluster without any typical time scale and amplitude, as we can see in Fig.5(a).

Enlarging the figure of the *halo* particle motions by ten times larger than the original one (Fig. 5(b)), we find the similar recurrent motions. The same pattern of motions is also found in the 100-times magnified figure (Fig.5(c)), although the lower cutoff effect is already observed in the recurrent time period. The repetition of the similar pattern suggests us a self-similar nested structure.

In order to analyze this behavior more quantitatively, we examine the frequency distribution of the recurrent time  $t_{\text{rec}} \equiv t_{\text{in}} - t_{\text{out}}$ , that is the time period from the moment  $t_{\text{in}}$  when one particle leaves the barycenter of the core to the moment  $t_{\text{out}}$  when it returns to the core and reaches the barycenter again. Here we defined the location of the barycenter of the core as

$$\theta_{bc} \equiv \sum_{i_c=1}^{N_c} \theta_{i_c} / N_c, \quad (4.9)$$

where  $\theta_{i_c}$  is the location of the  $i_c$ 'th particle in the *core* phase and  $N_c$  is the total number of the core particles at each moment.

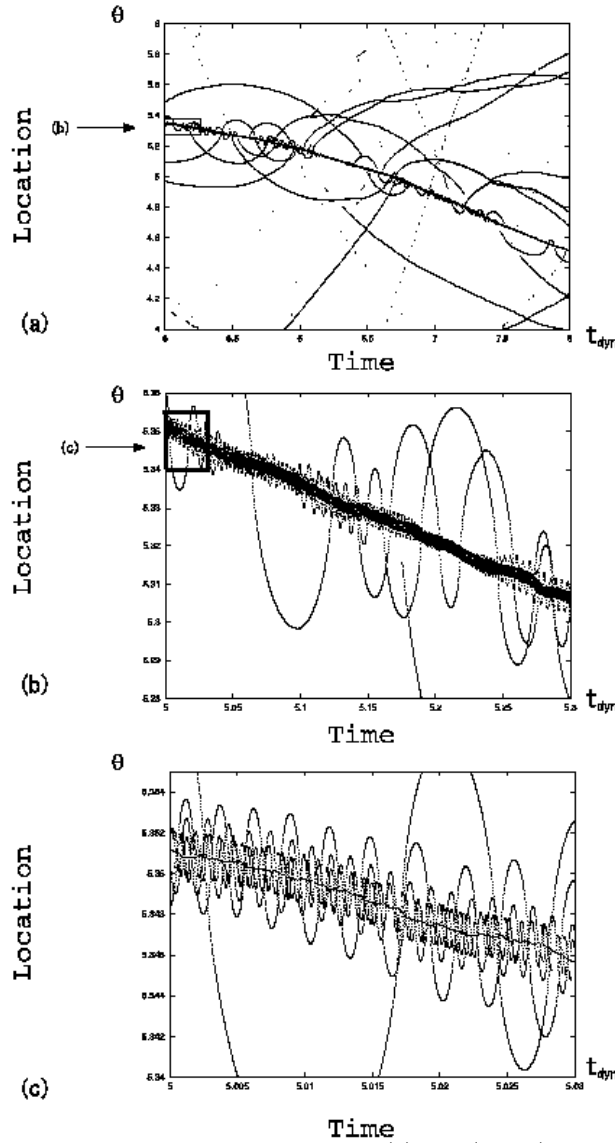


FIG. 5. Trajectories of *halo* particles for the time interval (a)  $t = (5 \sim 8) t_{\text{dyn}}$ , (b)  $t = (5 \sim 5.3) t_{\text{dyn}}$  and (c)  $t = (5 \sim 5.03) t_{\text{dyn}}$ . (b) and (c) are magnified figures of the squared region in (a) and (b), respectively. A self-similar nested structure is found.

In Fig.6, we depict the frequency distribution of recurrent time for the *core* particles and for the *halo*

particles. For *core* particles, as we expected, we find a peak in the distribution and a Gaussian-like fluctuation around its peak. The time scale at this peak position is related with the free-fall time  $t_{\text{cl-dyn}}$  defined in (2.5). On the other hand, for the halo particles, although a peak is found in the distribution, the distribution spreads very widely starting from the peak time interval and a long tail characterized by the scaling-law  $f(t_{\text{rec}}) \sim t_{\text{rec}}^{-p}$  is found. The value of  $p$  ( $\approx 2.0$ ) is almost independent of the value of the total energy  $U$  (Fig.7). This result is consistent with the motion of *halo* particles shown in Fig. 5, i.e. the self-similar nested structure. So we cannot identify the recurrent time scale for the halo particles with any characteristic time period against the case of the *core* particles. This makes it difficult to estimate the relaxation time not only for the halo particles but also for the whole system. We will see the effect of *halo* particles on the relaxation in §.VI.

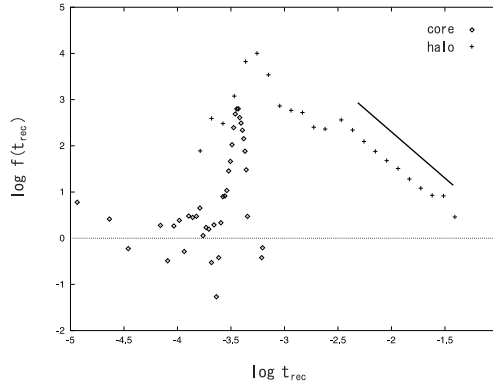


FIG. 6. Log-log plots of frequency distribution  $f(t_{\text{rec}})$  for *core* particles (cross) [(i)] and for *halo* particles (square) [(ii)], where  $t_{\text{rec}}$  is the recurrent time of each particle. The peak appears at  $t_{\text{rec}} \sim 10^{-3.5}t_{\text{dyn}} \approx 0.0003t_{\text{dyn}}$  and at  $t_{\text{rec}} \sim 10^{-3.15}t_{\text{dyn}} \approx 0.0007t_{\text{dyn}}$  in (i) and (ii), respectively, while the constant slope is seen only in (ii). The straight solid line represents the slope of  $-2.0$ .

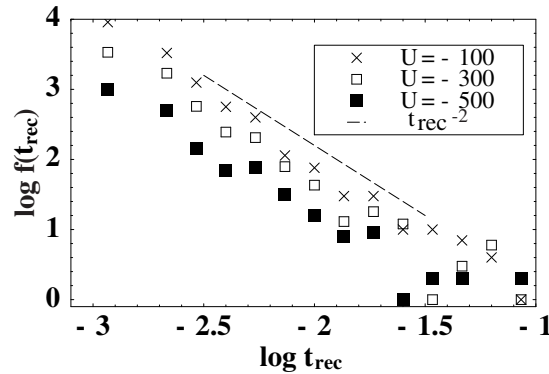


FIG. 7. Log-log plots of the frequency distribution  $f(t_{\text{rec}})$  for *halo* particles for several values of  $U$ . Each data shows the same slope within the range  $10^{-2.5}t_{\text{dyn}} < t_{\text{rec}} < 10^{-1.5}t_{\text{dyn}}$ . The straight line represents the slope of  $-2.0$ .

## V. FRACTAL ANALYSIS

In the previous section, we found that the velocity distribution of *halo* particles is non-Gaussian with the  $v^{-2}$ -tail and each *halo* particle moves recurrently without any typical time scale of oscillation. This recurrent motion also shows up the self-similar nested structure. We then expect that the *halo* particles may lead to the fractal structure in the particle distribution as well. In this section, we shall calculate the fractal dimension of the distribution with the box-counting method [24].

For this purpose, we first divide the total one-dimensional periodic distance  $2\pi R$  by many boxes with the size  $\ell$  and count the number  $N(\ell)$  of the box which contains at least one *halo* particle. Then we define the following quantity.

$$D(\ell) \equiv - \left\langle \frac{\partial(\log N(\ell))}{\partial(\log \ell)} \right\rangle_{\text{ens}}, \quad (5.1)$$

where,  $\langle \cdots \rangle_{\text{ens}}$  refers to the ensemble average over the samples with the same energy  $U$ . We have used the data of particle distributions on  $n_T$  time slices which divide the period between  $t = 2000t_{\text{cl-dyn}}$  and  $5000t_{\text{cl-dyn}}$  by equal time interval. In this period, the phase ratios  $\lambda_{\text{core}}$ ,  $\lambda_{\text{halo}}$ , and  $\lambda_{\text{gas}}$  almost attain to constant values.

If fractal structure exists,  $D(\ell)$  will become constant for a finite range of  $\ell_1 \leq \ell \leq \ell_2$ . As for the bounds  $\ell_1, \ell_2$ , we have theoretical limits. The averaged distance between *gas* particles is estimated as

$$d_{\text{gas}}(\epsilon) \approx \frac{2\pi R}{N_{\text{gas}}(\epsilon)}, \quad (5.2)$$

where  $N_{\text{gas}}(\epsilon)$  is the number of the *gas* particles which move independently of a cluster. If the box size  $\ell$  is larger than  $d_{\text{gas}}(\epsilon)$ , we expect  $D \approx 1.0$ , because almost all of the boxes contain at least one particle. On the other hand, if  $\ell$  is smaller than the cutoff distance  $\xi$ , we may lose the information about gravitational force, because in such a small scale, the *core* particles dominate and the interaction is no longer gravitational. Then the fractal structure caused by gravitational interaction, if it exists, will be found in some finite range of  $\ell_1 \leq \ell \leq \ell_2$  with  $\ell_1 > \xi$  and  $\ell_2 < d_{\text{gas}}(\epsilon)$ . In fact, in the case with  $\epsilon = 2.5 \times 10^{-7}$  and  $U = -100$ , we can see the typical behavior of  $N(\ell)$  as the function of  $\ell$  in Fig.8. In this picture, we can see the wide range of flat plateau corresponding to the small value of fractal dimension in the range of  $10^{-3}R < \ell < 10^{-1}R$ .

This fractal structure seems to originate in the *halo* particles, because the *halo* particles not only dominate in the above scale range but also show non-Gaussian feature and the self-similar jumps. If the fractal structure found above is really due to the *halo* particles, it is expected that such a fractal structure has its own origin at the barycenter of the core. In order to check whether this is true or not, we reanalyze the fractal dimension of the same data set in a different way. For the present purpose, we introduce a new coordinate  $\bar{\theta}$  as  $\bar{\theta} \equiv \theta - \theta_{bc}$  so as to relocate  $\theta_{bc}$  to the origin of the coordinate  $\bar{\theta}$ . Next we superpose the data on the different time slices  $t_k = t_0 + k\Delta t$  from  $k = 1$  to  $n_T$ , i.e.  $\{\bar{\theta}_i(t_k) | i = 1 \sim N, k = 1 \sim n_T\}$  and then calculate the fractal dimension. Moreover, we have to re-scale the angular variables as  $\bar{\Theta} \equiv n_T \bar{\theta}$  and calculate the fractal dimension as

$$D(\bar{L}) \equiv - \frac{\partial(\log \tilde{N}(\bar{L}))}{\partial(\log \bar{L})}, \quad (5.3)$$

where  $\bar{L}$  is the box size in the coordinate  $\bar{\Theta}$  and the  $\tilde{N}(\bar{L})$  is the number of the box which contains at least one particle for the superposed data. The reason is that the superposition of independent data will destroy the scaling behavior. Suppose that the distribution on each slice is described by the fractal structure with the dimension  $d$ , i.e.  $N(\bar{\ell}) = N_0 (\bar{\ell}/R)^{-d}$ . The probability that we find the filled box is  $p(\bar{\ell}) = N(\bar{\ell})/N_{\text{box}}(\bar{\ell})$  where  $N_{\text{box}}(\bar{\ell})$  is the total number of boxes with the size  $\bar{\ell}$ . Note that the scaling property in  $N(\bar{\ell})$  is valid only for  $\bar{\ell} < \bar{\ell}_{\text{max}} = (2\pi/N_0)^{1/(1-d)}R$  because  $p(\bar{\ell}_{\text{max}}) = 1$ . If we superpose  $n_T$  independent data, the probability that we find the unfilled box for such data is given by  $(1 - p(\bar{\ell}))^{n_T}$ . Then the probability for the filled box is  $1 - (1 - p(\bar{\ell}))^{n_T}$ , which gives us the number of the filled boxes with the size  $\bar{\ell}$  as

$$\begin{aligned}
N(\bar{\ell}) &= N_{\text{box}}(\bar{\ell}) \times [1 - (1 - p(\bar{\ell}))^{n_T}] \\
&= 2\pi \left(\frac{\bar{\ell}}{R}\right)^{-1} \times \left[1 - \left(1 - \frac{N_0}{2\pi} \left(\frac{\bar{\ell}}{R}\right)^{1-d}\right)^{n_T}\right].
\end{aligned} \tag{5.4}$$

The  $\bar{\ell}$  dependence of this function is rather complicated, but we can show that there is still the same scaling law such that  $N(\bar{\ell}) \sim \bar{\ell}^{-d}$  for much smaller box size, i.e.  $\bar{\ell} < (2\pi/N_0 n_T)^{1/(1-d)} R \ll \bar{\ell}_{\text{max}}$ . However, if we re-scale the angular coordinate as given in the above, that is, if we consider the rescaled box number of  $\tilde{N}(\bar{L}) \equiv N(\bar{L}/n_T)$ , the scaling range comes up to the original range of the fractal structure, i.e.  $\bar{L} < (2\pi/N_0)^{1/(1-d)} n_T^{-d/(1-d)} R \sim \bar{\ell}_{\text{max}}$  for small value of  $d$ . In fact, for the superposed data with  $n_T = 10$ , and 100, we find  $D(\bar{L}) \approx D(\bar{\ell})$  in almost the same range of the box-size (see Fig.8). This result confirms that the derived fractal properties certainly originate from the non-Gaussian motion of the *halo* particles around the barycenter of the cluster.

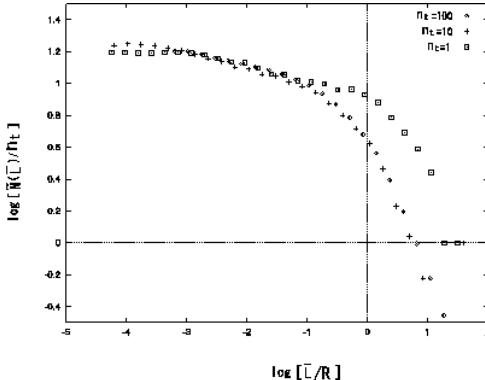


FIG. 8. Log-log plot for the box scale  $\bar{L}$  vs the number of the boxed occupied by at least one *halo* particle rescaled by  $n_T$  in the case with  $n_T = 1$ , and 10 ( $t_0 = 2.0t_{\text{dyn}}$ ,  $\Delta t = 0.3t_{\text{dyn}}$ ), and 100 ( $t_0 = 2.0t_{\text{dyn}}$ ,  $\Delta t = 0.03t_{\text{dyn}}$ ) for the cutoff  $\epsilon = 2.5 \times 10^{-7}$  where  $\xi \approx 10^{-3} R$ . The data points in these three cases are overlapped in the range of  $\xi < \bar{L} < 10^{-1} R$ . The fractal dimension  $D(\bar{L})$  derived from the slope in this range is 0.1.

The energy and cutoff dependencies of fractal dimension  $D$  are shown in Fig.9. Here we show the fractal dimension of *halo* particles in the energy range of both  $\mathcal{C}$ -state and  $\mathcal{V}$ -state. We find that the fractal dimension  $D$  is almost independent of the energy  $U$ , and as the cutoff  $\epsilon$  goes down,  $D$  gets lower but the range where  $D$  is constant becomes wider. On the other hand, in the limit of  $\epsilon \rightarrow 1$ , the fractal disappears, since the range of  $\xi < \ell < d_{\text{gas}}(\epsilon)$  becomes too narrow to exhibit the fractal structure.

In the limit of real gravitational interaction ( $\epsilon \rightarrow 0$ ), the state with negative specific heat appears in much wider energy range in which the fractal dimension is constant. This universality is likely to be independent of the temperature or the energy of the system. This is reminiscent of the SOC scenario which appears in the sand-pile experiment [19].

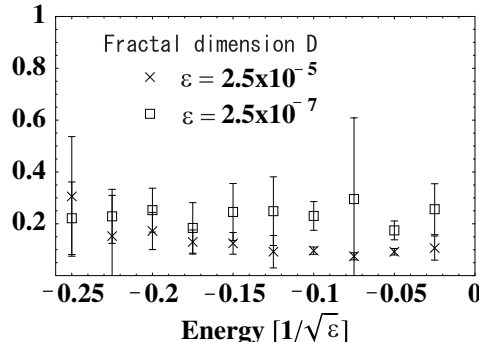


FIG. 9. The fractal dimension  $D$  vs the energy per particle  $U$ . For the convenience,  $U$  is rescaled by the  $\epsilon^{-1/2}$ . The case of  $\epsilon = 1.0 \times 10^{-5}$  (cross with error bars) and the case of  $\epsilon = 1.0 \times 10^{-7}$  (square with error bars) are plotted. It seems that the dimension  $D$  does not depend on  $U$ . Since the number of halo particles is small in the low energy, the error becomes large.

## VI. RELAXATION

One of the most important issue in statistical physics of  $N$ -particle system is relaxation. In order to study such a relaxation process of our model, we choose several different initial conditions for the same values of  $\epsilon$  and  $U$ . Here we have examined two models, i.e. (i)  $\epsilon = 2.5 \times 10^{-3}, U = -0.65$  and (ii)  $\epsilon = 2.5 \times 10^{-7}, U = -100$ , for both of which a negative specific heat appears. As for initial conditions, we locate several clusters at the same interval, each of them is composed of the same number of particles located at the same position. The number of clusters is chosen as 5, 10, 20, 25, and 50 for the model (i) and 5, 10, 20, and 25 for the model (ii). The initial velocities of particles are given randomly, so as to make the total energy the same value,  $U = -0.65$  for (i) and  $U = -100$  for (ii).

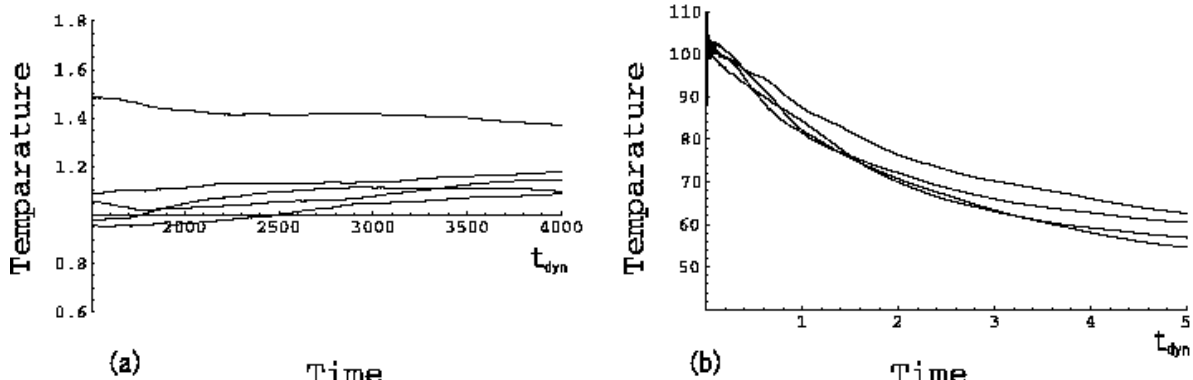


FIG. 10. The time variation of temperature for the different initial conditions with the same energy and with the same value of cutoff. (a) is the case with (i)  $\epsilon = 2.5 \times 10^{-3}, U = -0.65$  and (b) is the case with (ii)  $\epsilon = 2.5 \times 10^{-7}, U = -100$ . Temperatures for all of the initial conditions seem to converge to the same value in (a), while they do not in (b).

The time series of the temperature for these initial conditions are depicted in Fig.10. In the case of (i), the temperatures seem to approach the same value, although each of them does not yet converge to a constant value. On the other hand, in the case of (ii), each temperature seems to converge to a constant value, although those values are different. This can be easily explained by the difference of the ratio  $t_{\text{cl-dyn}}/t_{\text{dyn}}$  between the two models. (Remember that  $t_{\text{cl-dyn}}/t_{\text{dyn}} = 10$  and 0.004 for (i) and (ii), respectively.) We stop our calculations at the same time interval in the unit of  $t_{\text{cl-dyn}}$  because we may need more CPU time for further calculation.

The rapid convergence of each temperature in (ii) means that the local relaxation in each cluster is much faster than that in (i). On the other hand, the tendency of global relaxation can be found only in (i). This is just because the total time interval of simulation in (i) is  $4000t_{\text{dyn}}$ , which is 1000 times longer than the time interval with the same unit in (ii). In the case of (ii), We can extrapolate those curves in Fig 10 and naively obtain the relaxation time as  $t_{\text{relax}} \sim 10^4 t_{\text{dyn}}$ .

There may be another indicator to see the relaxation process, which is a convergence of each  $\lambda$ . If the system is completely relaxed, the ratio of each phase may approach the same value for any initial conditions. In fact, this seems true from our numerical simulation, especially for the case (i). Then we shall show the convergence of each  $\langle \lambda \rangle$  in Fig. 11. Here,  $\langle \lambda \rangle$  denotes the time averaging of  $\lambda$ . We find the similar difference between the two cases in the time series of  $\langle \lambda \rangle$ . In the case (i),  $\langle \lambda_{\text{gas}} \rangle$  converges

to the same value independent of initial conditions within the range of the calculation, while the others have not converge for different initial conditions, but seem to be approaching the same value. In the case of (ii), on the other hand, only  $\langle \lambda_{core} \rangle$  converges to the same value, while  $\langle \lambda_{halo} \rangle$  and  $\langle \lambda_{gas} \rangle$  are converging to the different values depending on the initial conditions. These results support our above statement that the local relaxation in the case (ii) is much faster than that in the case (i), since the *core* particles mainly contribute to such a relaxation.

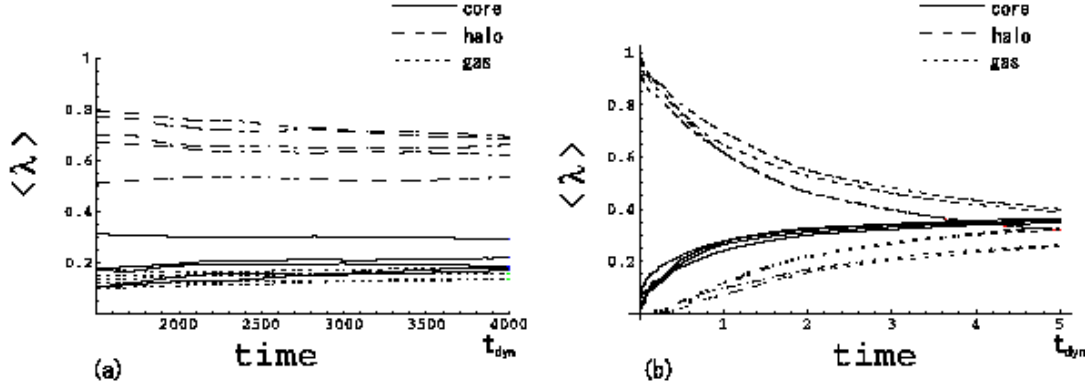


FIG. 11. The time variation of  $\langle \lambda \rangle$  for the same initial conditions as in Fig.8. In (a),  $\langle \lambda_{gas} \rangle$  converges to the same value and the others also seem to be approaching the same value. In (b), on the other hand, only  $\langle \lambda_{core} \rangle$  converges to the same value.

In the case of (ii), we also examine the time series of time-averaged kinetic energies per one particle for *core*, *halo* and *gas* particles, separately, defined by the similar equation to the right side of (3.1). As is seen in Fig. 12, the averaged kinetic energy for the *halo* particles fluctuates a lot comparing to those for other particles, which prevents us from defining the temperature for *halo* particles as (3.1). This is consistent with the results of velocity distributions in Fig.4.

By combining these results with the results in the previous section, we conclude that the particle motions in the *halo* phase play a key role in preventing the global relaxation, especially when the cutoff scale is much shorter than the radius.

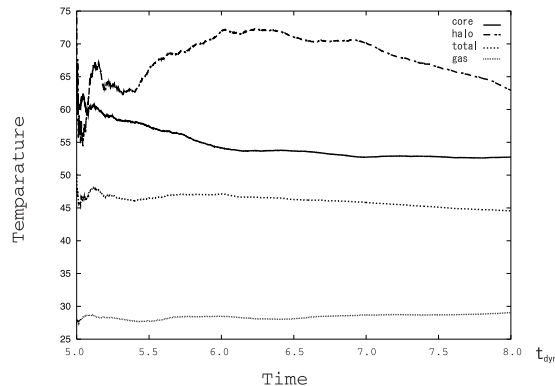


FIG. 12. The time variation of temperatures defined from the averaged kinetic energy for *core*, *halo*, and *gas* particles. The temperature defined by all particles is also shown. The kinetic energy of *halo* particles fluctuates around the averaged value too largely to define the temperature by the dispersion of velocity distribution. Here we take the time averaging for the time interval of  $5t_{dyn} < t < 8t_{dyn}$  in order not to pick up any initial transient effect.

## VII. CONCLUSION

In this paper we have studied the SGR model which is a one-dimensional toy model of a self-gravitating system. Although the system is one-dimensional, the force acting on the particles constrained on a circular ring is the conventional 3D gravitational interaction. As a result, in the microcanonical system, a negative specific heat appears and a phase transition occurs at low temperature. We introduce a short-range cutoff  $\epsilon$  so as to prevent the system from collapsing.

Using this SGR model, we have examined characteristic properties of a self-gravitating system such as a fractal structure and non-Gaussian velocity distribution, and analyzed the origin of these characteristic properties from the viewpoint of the gravitational phase transition.

We find that a virialized state with negative specific heat appears at the intermediate energy scale, where a phase transition occurs and a cluster is formed. Classifying the particles in each state into three phases (*core*, *halo* and *gas* phases), we can characterize this virialized state by non-thermal property of the particles in *halo* phase. We have then analyzed the motion of *halo* particles and its fractal structure. We find that the velocity distribution of a cluster in a virialized state is non-Gaussian with the  $v^{-2}$  tail. The *halo* particles also move recurrently without any typical time scale of oscillation. We also find the fractal structure of the *halo* particles in the  $\mathcal{V}$ -state with a box-counting method. The fractal dimension is rather small and depends on the cutoff. In the gravitational limit,  $\epsilon \rightarrow 0$ , the energy range with negative specific heat becomes broad, and the fractal structure becomes more prominent, although the dimension decreases.

As for the relaxation of the system, we can distinguish the local relaxation time from the global one. As the value of  $\epsilon$  gets smaller, the former time scale becomes shorter than the latter one. In this local relaxation time scale, the particles in *halo* phase fluctuate so largely that the equilibrium state is still quite far from the thermal-equilibrium state. So we find that the system remains in the quasi-equilibrium state characterized by scale-free *halo* particle motions during a long time interval for the small value of  $\epsilon$ . This quasi-equilibrium state keeps the memories of the initial conditions as is shown in sec.IV, which is reminiscent of the violent relaxation process [25]. This sort of quasi-equilibrium state could be characterized by the exotic statistics like Tsallis statistics [26] beyond the Maxwell-Boltzmann statistics.

In the limit of the real 3D gravitational force ( $\epsilon \rightarrow 0$ ), we find many universal features, the state with negative specific heat, non-Gaussian velocity distribution, and the fractal structure of the *halo* particles. Those are likely to be independent of the temperature or the energy of the system. This is reminiscent of the SOC scenario which appears in the sand-pile experiment [19]. The first order phase transition occurs even in the system with short range interactions as is seen in [14]. However, the above SOC type universal character could be the peculiar one which distinguishes the systems with the long-range interactions such as the gravitational force from those with the short range interactions. In two or three dimensional cases, it would be easy to compare the case with short-range interactions to the case with long-range ones, since the first order phase transition occurs in the former case. This would be our future work.

Our results could also give a hint for the mechanism of the observed universal character of gravitationally virialized objects such as molecular clouds. These statistical approach characterized by the SOC-type criticality could be the alternative standpoint to explain the universal nature of molecular clouds, such as fractal and Lévy type motion.

## ACKNOWLEDGMENTS

We would like to thank A. Nakamichi, I. Joichi, K. Nakamura and M. Hotta for useful discussions and comments. This work was supported partially by a Grant-in-Aid for Scientific Research Fund of the Ministry of Education, Science and Culture (Specially Promoted Research No. 08102010), and by the Waseda University Grant for Special Research Projects.

---

[1] W. H. Zurek, P. J. Quinn, J. K. Salmon, and M. S. Warren, *Astrophys. J.* **431** (1994), 559.

[2] F. Sylos Labini, M. Montuori and L. Pietronero, *Phys. Rep.* **293** (1998) 61.

[3] G. de Vaucouleurs, *Science* **167** (1970), 1203.

[4] R.B. Larson, *Mon. Not. R. astr. Soc.* **194** (1981), 809.

[5] E. Falgarone, T.G. Phillips and C.K. Walker, *Astrophys. J.* **378** (1991), 186.

[6] *Fluid Dynamics Stability and Turbulence*  
(T. Kambe and P.G. Drazin, University of Tokyo Press, 1998).

[7] F. Combes, *Proceedings of The Chaotic Universe Roma colloquium*,  
(World Scientific Advanced Series in Astrophysics and Cosmology, 1999)  
ed. V. Gurzadyan, Li-Zhi Fang and R. Ruffini.

[8] H.J. de Vega, N. Sánchez and F. Combes, *Phys. Rev.* **D54** (1996), 6008.

[9] V. A. Antonov, *Vest. leningr. gos. univ.* **7** (1962) 135.

[10] D. Lynden-Bell and R. Wood, *Mon. Not. R. astr. Soc.* **138** (1968) 495.

[11] I. Hachisu and D. Sugimoto, *Prog. Theor. Phys.* **60** (1978) 123.

[12] E. B. Aronson and C. J. Hansen, *Astrophys. J.* **177** (1972) 145.

[13] T. Padmanabhan, *Phys. Rep.* **188** (1990), 285.

[14] P. Hertel and W. Thirring, *Annals of physic.* **63** (1971), 520.

[15] A. Compagner, C. Bruin, and A. Roelse, *Phys. Rev.* **A39** (1989), 5989.

[16] G. L. Camm, *Mon. Not. R. astr. Soc.* **110** (1950), 305

[17] T. Tsuchiya, N. Gouda and T. Konishi, *Phys. Rev.* **E53** (1996), 2210.

[18] Y. Aizawa, K. Sato, and K. Ito, *Prog. Theor. Phys.* **103** (2000) 519-540.

[19] *Self-Organized Criticarity* (H. J. Jensen, Cambridge University Press, 1998).

[20] *An Introduction to Probability Theory and Its Applications* 2nd ed.  
(Wiley and Sons, Inc. New York, 1966), Vol. II.

[21] M. Antoni and S. Ruffo, *Phys. Rev.* **E52** (1995), 2361.

[22] M. Suzuki, *Phys. Lett. A* **146** (1990), 319.

[23] V. Latora, A. Rapisarda and S. Ruffo, *Phys. Rev. Lett.* **83** (1999), 2104.

[24] K. Falconer, *Fractal Geometry* (1990, John Wiley & Sons).

[25] D. Lynden-Bell, *Mon. Not. R. astr. Soc.* **136** (1967), 101.

[26] C. Tsallis, *Braz. J. Phys.* **29** (1999), 1.

